applied sciences

MDPI

Article

Development of Polymer-Cored Akaganeite Adsorbent for Phosphate Adsorption

Jiyeol Bae [1,2,†], Hyobin We [3,†], Suho Kim [1], Sungjik Oh [1] and Soyoung Baek [1,*]

[1] Department of Environmental Research, Korea Institute of Civil Engineering and Building Technology (KICT), Goyang 10223, Republic of Korea; baejiyeol@kict.re.kr (J.B.)
[2] Civil and Environmental Engineering, University of Science and Technology (UST), Daejeon 34113, Republic of Korea
[3] Atmospheric Environment Team, Gyeonggi Province Institute of Health and Environment Northern Support Institute, Uijeongbu-si 11780, Republic of Korea
* Correspondence: soyoung@kict.re.kr
† These authors contributed equally to this work.

Abstract: Environmental issues related to phosphate and resource depletion have recently emerged as serious problems. This study focuses on solving the problems of phosphate removal and recovery using synthesized granular akaganeite (GAK). This study identified that akaganeite, which possesses an FeOOH structure in iron oxyhydroxide, can be synthesized and used as a reusable material. Immobilization with the core–shell method using polyethersulfone was applied as a strategy to recover phosphate anions from a trace of phosphate solution. GAK was successfully analyzed using SEM/TGA/BET to understand its physical properties. XRD and SAD pattern analyses suggested that the GAK powder form was amorphous in nature. The powdered akaganeite had a surface area of 231 mg^2/g and a maximum adsorption capacity of 21.27 mg/g. To prevent the dispersion of powder during granulation, polyethersulfone was used as a scaffold since akaganeite particles can be effectively immobilized onto PES polymer scaffolds, as substantiated by the SEM/EDS results. Moreover, a lack of changes in the pore sizes suggested that physical properties remained unchanged. Furthermore, compared to the granular akaganeite, the surface area of powdered akaganeite decreased 4–5-fold. The adsorption kinetic of granular akaganeite fit the pseudo-second-order model. The powdered form displayed high removal efficiency, intimate with phosphate anions, when $n > 1.0$, instead of lower K_F. On the other hand, granular akaganeite showed lower affinity when $n < 1.0$, but appeared positive for an adsorbate with higher KF. This implies that the granulation of akaganeite with the PES polymer did not change its adsorption property, with the maximum adsorption capacity for granular akaganeite being 3.65 mg/g.

Keywords: polymer core granulation; phosphate removal; akaganeite adsorbent

Citation: Bae, J.; We, H.; Kim, S.; Oh, S.; Baek, S. Development of Polymer-Cored Akaganeite Adsorbent for Phosphate Adsorption. *Appl. Sci.* **2024**, *14*, 146. https://doi.org/10.3390/app14010146

Academic Editor: Domenico Lombardo

Received: 8 November 2023
Revised: 18 December 2023
Accepted: 21 December 2023
Published: 23 December 2023

1. Introduction

Phosphorus is commonly found in many terrestrial and aquatic areas where it acts as an essential nutrient for the growth of plants, animals, bacteria, and soil-based organisms. Owing to this, fertilizers containing phosphate have been used in agricultural production for many years. Moreover, inorganic phosphate-based products have been used in practical applications, including toothpaste, cosmetics, synthetic detergents, bone cement, and medical products [1–6].

The increasing consumption of phosphates has led to two significant problems. First, phosphate rock, which contains high amounts of phosphate, is a limited global resource. With the increasing global phosphate consumption, the prices of phosphate rock have been climbing in the mineral market. In fact, global phosphorus reserves likely peaked, causing greater derived demand for phosphate rock [7]. The Food and Agricultural Organization of the United Nations (FAO) reported that demands for fertilizers increased by approximately

2.6% each year from 2010 to 2014 [8]. Based on this price inflation, further investigations have revealed that the rising demand for phosphate rock will continue to deplete phosphate resources in the future. In addition, investigators predict that given the current phosphate usage in America and China, their resources are expected to be depleted by 2070 [9]. Furthermore, an overload of waste phosphorus from sewage treatment plants directly damages aquatic systems, causing excessive microbial growth in developed cities. It is difficult to safely remove this wastewater, including phosphate, from sewage treatment plants; typical plants employ only biological processes, making it hard to remove traces of phosphate.

The overconsumption of phosphates creates two main problems: on a smaller scale, it influences aquatic systems, and on a larger scale, it depletes phosphate reserves. These increasingly problematic issues have garnered international attention. A more gradual use of this resource will put pressure on conservation and environmental protection efforts.

Recently, municipal sewage treatment plants have started making an effort to remove phosphates by incorporating a variety of chemical and precipitation methods. The most commonly used method is the use of coagulants, such as inorganic coagulants of Al^{+3} and Fe^{+2}, to settle the precipitation [10]. However, such chemical dosing generates by-products and disposal problems given the nonrecovery of phosphorus. Thus, to address this problem, a crystallization technique with magnesium dosing has been introduced for removing ammonium from wastewater and obtaining the nutrient elements struvite and apatite [11]. Though this technique has improved the recovery of coagulated phosphorus, it has failed to recover the phosphate resources. However, it is still difficult to remove the precipitate containing the phosphorus from the bottom of the grit chamber. The powdered chemical products used in most of these techniques cause fine particles to be dissolved in water, which are released from effluent sewage treatment plants. These secondary pollutants were first reported in Korean rivers by the National Institute of Environmental Research of Korea [12]. Three factors are essential for overcoming these problems: developing high removal capacity with economics, developing reusable materials with recovered phosphorus, and immobilizing fine particles to prevent secondary pollution.

Iron-based adsorbents are particularly useful because they are safe and economical. Iron-based adsorption studies have received significant, sustained attention for many years now. Many long-term studies have verified that iron-based adsorbents are capable of removing various heavy metals [13–18]. They exist in various forms and have varied properties, and they can be classified as iron oxides, iron hydroxides, or iron oxyhydroxides, depending on their characteristics [19,20]. Among them, iron oxyhydroxide is well known for adsorbing anionic substances. However, the reusability of the material depends on its specific characteristics or adsorption mechanism impacts [21,22]. Thus, this study used iron oxyhydroxide adsorbents to recover reusable phosphorus.

In previous studies, powder forms of akaganeite were evaluated for the removal of oxyanions such as phosphate [19,20]. However, the use of powdered adsorbents in water treatment is problematic, e.g., due to the need for posterior removal of fine adsorbent particles from the purified water. Applications where powdered adsorbents are encased in the filtration columns require a high working pressure. Thus, in order to solve this problem fundamentally, the powdered adsorbents need to be immobilized, and immobilizing a powdered adsorbent onto a polymer scaffold can be a good way. Various immobilization techniques have been introduced and are being widely used for adsorption, acting as a catalyst, in the medical field [23–26]. Granulation is an important component of the adsorption process where nanoparticles are immobilized from the scaffold material and are directly put in contact with targeted anion materials on the edge of the beads. Polyethersulfone (PES) polymers, as organic compounds, have been found to be suitable for immobilizing fine particles; they provide an optimal material that is non-toxic and freely forms a shape given the high viscosity of the liquid. Moreover, the material is highly resistant to acidic and alkaline conditions and has superior strength in the membrane field [27]. In terms of

recovering phosphorus from sewage treatment plants, these two strategies are extremely close to being successful and have the potential to relieve the environmental burden.

In this study, phosphate removal and recovery were accomplished by using akaganeite, which is an iron oxyhydroxide polymorph. This study allowed the identification of adsorbents that could be used to recycle phosphate. Granular iron oxyhydroxides were synthesized using a simple core–shell technique using the PES polymer as a scaffold. Immobilizing the nanoparticles on the surface of the beads is important because it increases the effective area for removing phosphate anions on granular adsorbents. Therefore, we attempted immobilizing nanoparticles on the outer surface using granular adsorbents. First, the characteristics of powdered iron oxyhydroxide were analyzed. To determine its adsorption, tests were conducted on the phosphate anion (PO_4^{3-}; as HPO_4^{2-} and $H_2PO_4^-$ at near-neutral pH) using isotherm adsorption, kinetic adsorption and desorption, the effects of pH, and regeneration experiments for granular forms. Based on these results, this study investigated the formation of struvite using eluted phosphorus and evaluated the application of granular iron oxyhydroxide to water treatment technology.

2. Materials and Methods

2.1. Preparation of Powdered Iron Oxyhydroxide

2.1.1. Materials

All chemicals in this study were of reagent grade and used without further purification. Sodium hydroxide (NaOH) and ammonium carbonate (NH_4OH) were purchased from Sigma-Aldrich. Iron species reagents purchased were as follows: Iron (III) sulfate pentahydrate ($Fe_2(SO_4)_3 \cdot 5H_2O$) from Acros Organics in Germany; Iron (III) chloride hexahydrate ($FeCl_3 \cdot 6H_2O$) from Fluka in Germany; and Iron(II) nitrate 9-hydrate ($Fe(NO_3)_3 \cdot 9H_2O$) from Yakuri Pure Chemical Ltd. in Kyoto, Japan. Urea (H_2NCONH_2) and ethylene glycol ($C_2H_6O_2$) were purchased from Daejung in the Republic of Korea. Polyethersulfone (Gafone 3000) was obtained from Solvay Advanced polymers, and Dimethylformamide (DMF) was purchased from Sigma-Aldrich (St. Louis, MO, USA).

2.1.2. Synthesis of Iron Oxyhydroxide Adsorbents

A total of 0.1 M of the ammonium carbonate solution (2000 mL) was added dropwise with constant vigorous stirring to 0.1 M ferric chloride solution (2000 mL). The generated brown precipitate was then washed thrice with 2000 mL of deionized (DI) water and separated by centrifugation at 2000 rpm for 10 min. Since the radius of the centrifuge rotor used in the centrifugation process is 5 cm, the relative centrifugal force applied in this process is $224\times g$. The final products were stored in an oven at 55 °C for 48 h and then washed with DI water.

2.2. Granulation of Powdered Adsorbents

To immobilize particles, 20% PES polymer solution was prepared by dissolving 6 g of polyethersulfone in 24 mL DMF solution. Later, the PES polymer solution was stored at 150 rpm for 24 h in a shaking incubator at room temperature. The PES polymer solution was dropped onto powdered materials via a syringe. A drop of translucent PES polymer on the plate was shaken until powdered akaganeite was covered with PES (Figure 1). Each drop that fell in DI water was indurated. After separation from DI water, sphere-shaped akaganeite was obtained (Figure 1).

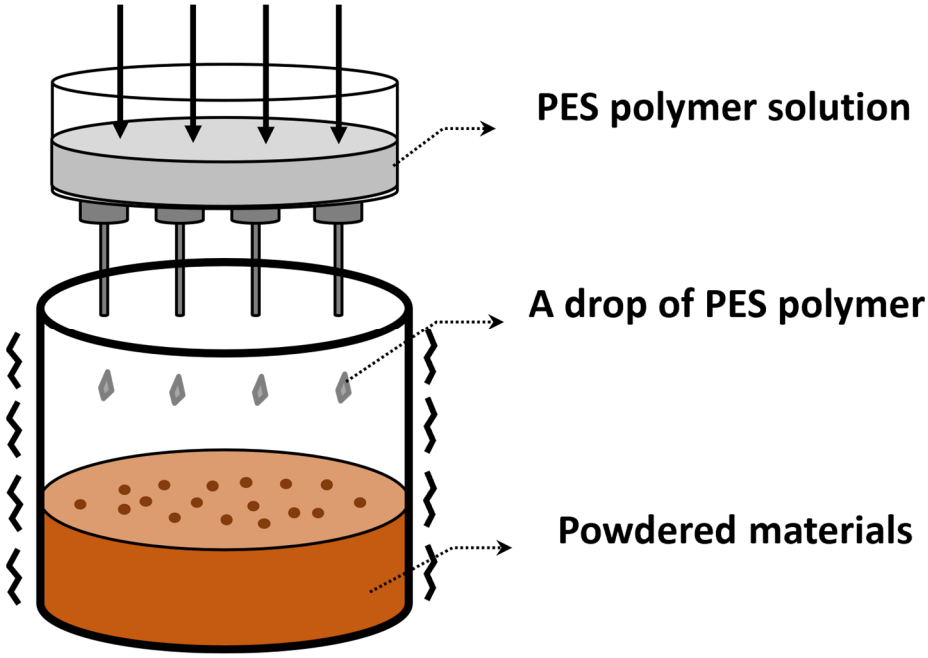

Figure 1. Schematic diagram of granulation process using PES polymer.

2.3. Characterization

2.3.1. X-ray Diffraction (XRD) Analysis

XRD patterns were measured using an X-ray diffractometer (X'Pert PRO Multi-Purpose X-ray Diffractometer, PANalytical) using Cu Ka radiation at 40 kV and 25 mA, with a wavelength equal to 1.5405980 Å. A sample of goethite, which has an orthorhombic structure, was recorded at scan speed of 1°/min at low 2θ angles from 20 to 80°. A sample of akaganeite, which has a tetragonal structure, was recorded at a scan speed of 1°/min at low 2θ angles from 10 to 40°. Finally, a sample of lepidocrocite, which has an orthorhombic structure, was recorded at a scan speed of 1°/min at low 2θ angles from 20 to 80°. The samples were then analyzed using selected area diffraction (SAD) patterns. The standard data were obtained from the International Centre for Diffraction Data (Goethite, ICDD No. 98-015-9962; Akaganeite, ICDD No. 96-900-1320; Lepidocrocite, ICDD No. 98-010-8876).

2.3.2. Transmission Electron Microscopy (TEM) Analysis

Powdered samples were prepared by dispersing them in ethanol and dried on a Cu grid coated with carbon film. Field emission transmission electron microscopy (JEM-2100F, JEOL, Peabody, MA, USA) was performed to obtain TEM images.

2.3.3. Nitrogen Adsorption–Desorption Measurement

Nitrogen adsorption–desorption measurements were performed at 77 K on a Micromeritics ASAP 2020 analyzer. A sample of powdered goethite was degassed for 24 h at 150 °C, while a sample of powdered akaganeite was degassed for 16 h at room temperature; a sample of powdered lepidocrocite was degassed for 20 h at 80 °C. Each sample of granular iron oxyhydroxide was degassed under the same conditions as those for each powdered iron oxyhydroxide sample. Then, the samples were analyzed using the Barett–Joyner–Halenda (BJH) method. The adsorption pore size distribution (PSD), which is based on nitrogen adsorption isotherms, was calculated. Additionally, the pore volume was obtained at the $P/P_0 \leq 0.976$ single point, and BET surface area was calculated from adsorption data.

2.3.4. Isoelectric Point Measurement and Zeta Potential Measurement

The point of zero charge pH (pH_{pzc}) for each powdered iron oxyhydroxide was determined using a zeta potential analyzer (Nano ZS, Malvern, Chester County, PA, USA).

Each iron hydroxide sample of 0.5 g/L was suspended in 0.01 M $NaNO_3$ solution (50 mL) as an electrolyte, and the aqueous suspension was equilibrated at different pH values using the HCl and NaOH solutions. The average zeta potential at a certain pH value was plotted on pH in the range from 3 to 11.

2.3.5. Scanning Electron Microscopy (SEM) Analysis

The cross-section of the granular iron oxyhydroxide was observed using a field emission scanning electron microscope (S-4700, Hitachi, Tokyo, Japan). Each sample was divided into blank, 30, 60, 120, 300, and 1440 s exposure times in air. All measurements were performed at 10 kV. An energy-dispersive X-ray spectrometer (EDS) was also used to confirm the chemical constituents of the surface. EDS analysis and the analysis of the distribution of Fe on the PES were conducted with a spot with an approximate diameter of 20 μm in selected areas on the sample.

2.3.6. Thermogravimetric Analysis (TGA)

The weights of each powdered and granular iron oxyhydroxide required for immobilization on the PES polymer were analyzed with increasing temperature using a thermogravimetric analyzer (TGA 2050, TA instruments, New castle, DE, USA) under a nitrogen flow of 100 mL/min.

2.4. Adsorption/Desorption Experiments

Batch Experiment

A series of batch experiments were conducted to evaluate the performance of the new material in terms of regeneration and removal of aqueous phosphate. Isothermal adsorption was conducted by adjusting the concentration of phosphate for powdered/granular adsorbents. Additionally, the kinetic experiment of adsorption/desorption was conducted with increasing time for powdered/granular adsorbents. The pH effect experiment was performed by adjusting the pH using HCl and NaOH solutions for the granular adsorbent. The desorption experiment was performed using NaOH 0.5 M solution for 6 h by injecting the adsorbent adsorbed from phosphate for granular adsorbents. Finally, 10-cycle regeneration was conducted through continuous adsorption/desorption experiments. During the regeneration experiments, the adsorbents were washed with DI water following the desorption, before the adsorption step was started again. All of the adsorption experiments were carried out in a 50 mL conical tube containing 50 mL of phosphate solution (initial concentration: 5 mg/L, except isothermal adsorption experiment) and 0.05 g of the powdered/granular adsorbents. All of the samples were then shaken at 150 rpm/min in a shake incubator at 25. Samples were filtered through a 0.2 μm cellulose acetate membrane filter, extracted by solid-phase extraction, and analyzed using the UV spectrum (HS-3300, HUMAS, Daejeon, Republic of Korea).

3. Results and Discussion

3.1. Characteristic Analysis of Iron Oxyhydroxide Material

3.1.1. XRD Analysis of Powdered Iron Oxyhydroxide

The XRD patterns of the synthesized iron oxyhydroxide nanoparticles are presented in Figure 2. The diffraction peaks obtained from the XRD analysis of FeOOH nanoparticles were compared with the standard database (The International Centre for Diffraction Data (ICDD), 1997) using PCPDFWIN Version 2.00 software. The red color lines indicate reference peaks applicable to each nanoparticle, as provided by ICDD. For synthesized akaganeite data, the 203 hkl peak displayed weakening intensity against the reference data, indicating that the lattice plane of 203, 200, 001 hkl in a unit cell showed amorphous structure responding to the weak diffraction from constructive interference by an irregular structure. A peak of 312 hkl with relatively strong intensities can suggest that the akaganeite phase formed at a length perpendicular to 312 hkl.

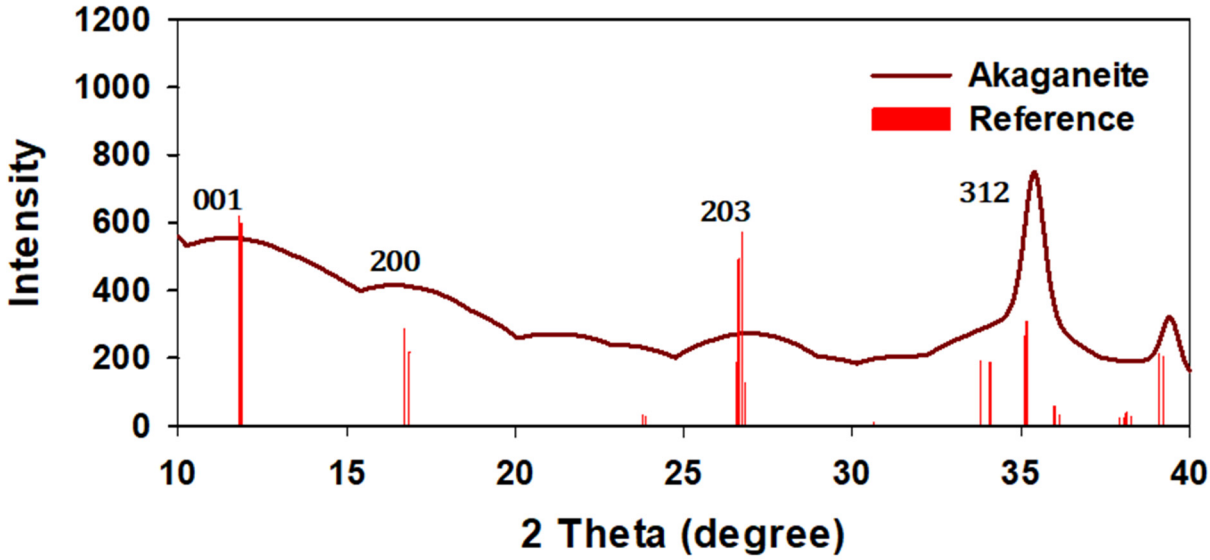

Figure 2. The diffraction peaks obtained from each iron akaganeite with those of the standard database (red).

3.1.2. Transmission Electron Microscopy (TEM) Analysis of Powdered Iron Oxyhydroxide

The morphology and crystallinity of each iron oxyhydroxide were investigated through TEM, as shown in Figure 3. The shape of goethite resembled a long stick, as mentioned in the XRD analysis. The goethite particle was over 200 nm in length and was confirmed to have crystallinity through SAD. For akaganeite, XRD showed particles similar to aggregated millet grains having an average size of 5 nm. SAD patterns for akaganeite indicated an amorphous phase, as seen in the XRD data of akaganeite. Overall, the study suggests that akaganeite appears to have a different phase and has a rod shape, which is a result of a blunt shape due to a noncrystalline structure. Lepidocrocite develops in a flower shape (Figure 3). The phase appears as flakes with very sharp tips, and the particles were observed in aggregation. The crystallinity of lepidocrocite was confirmed through SAD patterns. The lepidocrocite particles had a size of approximately 5–10 nm, and the size of the extended stem on the particle was less than 200 nm in length.

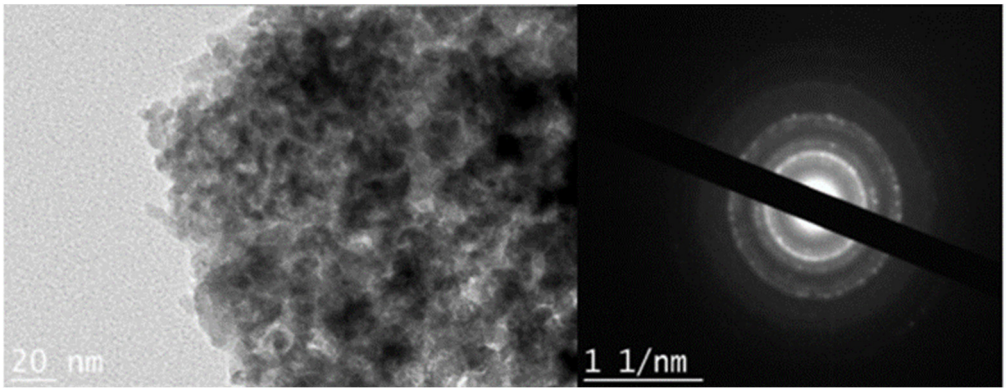

Figure 3. TEM images and selected area diffraction (SAD) patterns of akaganeite.

3.1.3. BET Analysis and Zeta-Potential Analysis of Powdered Iron Oxyhydroxide

The akaganeite had a higher BET surface area (231 m^2/g) than other materials. When considering the pore size and volume, the effective area of akaganeite is advantageous for adsorbing polluted substances with regard to contact between anions and those surfaces. This may be attributed to akaganeite forming a tunnel structure in a unit cell [28]. Meanwhile, akaganeite PZC was observed to have a higher pH (pH 10) than general oxyhydroxide (pH 7~9) [29]; lepidocrocite PZC had a pH of 9.5. Phosphate has a natural pH of

5~10 mg/L; thus, the zeta potential of akaganeite in the range of pH 6–7 is advantageous for adsorbing phosphate anions by attracting electrostatic force. Iron oxyhydroxide is known for adsorption via electrostatic forces or chemisorption. Chemisorption implies that it does not return to its original state on bonding with other anions. In the absence of this, it is acted upon by electrostatic forces from anions of hydroxyl groups, thus helping the desorption of the anion by switching the O^- on the FeOOH surface [21]. Further investigations are required to understand interfacial behavior in order to distinguish the types of bonds. This study attempted to understand the sorption behavior by conducting repetition tests on these powders.

3.2. Granulation of Akaganeite

3.2.1. Optimum Granulation Condition for Iron Oxyhydroxide Powder

Time variation with PES polymer exposure to the air during the process of granulation was monitored, and corresponding SEM images of cross-sections were obtained. Only granular PES without powdered akaganeite showed that bulky pores were located in internal granules and fine pores were located at the edge (Figure 4a). SEM images (b)–(f) suggest that powdered akaganeite was immobilized around the edge of the PES polymer. Though (a) and (b) appear similar, the latter has a rough surface on the edge when compared to blank (a), where the powdered akaganeite attaches to the PES polymer. With increasing the exposure time, a pore in an internal granule was converted to a huge hole, and the akaganeite layer formed a thin layer (Figure 4b–f). The reason for phase inversion has been attributed to the non-solvent/solvent exchange rate, with DI water as the non-solvent and the DMF as the solvent; this parameter plays the role of drying phase inversion phenomena that control the phase of the PES polymer in a membrane field [30]. The DMF solvent dissolved in water when immersed, and the position was filled with water by allowing water to form empty pores in the internal PES. Moreover, images (b)~(f) explain why more pores were produced with decreasing exposure time and the non-solvent/solvent exchange rate of water was faster than that of natural volatilization. These results suggest that a granule with much higher exposure time had a big hole, not a pore, and that the drying phase inversion did occur, which did not allow PES enough time to form pores (f); thus, PES polymer formed a much denser non-porous structure. Because of this, a granule of (f) must form a hole in the internal granule. As a result, granular akaganeite at 30 s of exposure time, which does not float on water, was selected and carefully analyzed.

To analyze the components of the granule surface, an edge was analyzed through field emission scanning electron microscopy with energy-dispersive X-ray spectroscopy (FESEM-EDS). Akaganeite formed the chemical constituents of $FeOOH{\cdot}H_2O$ (Fe 52.2%, H_2O 25.0%) [22], and polyethersulfone was used to immobilize particle forms ($C_{12}H_8O_3S$) [31].

According to the results obtained from qualitative analysis (Table 1), the S element existed only in the PES polymer, not in akaganeite. Thus, the S element can be a reference for the existence of PES. In order to measure the distribution of akaganeite powder in the akaganeite granule, EDS mapping was performed on the surface of the granule where the akaganeite was immobilized (#1 in Figure 5b) and the inside of the granule (#2 in Figure 5b). The O and Fe contents in #1 were higher than those in #2 (Figure 5a,b). Moreover, the EDS mapping results (red dot in (b) and white dot in (c) in Figure 5) confirmed that the Fe and O elements were situated close to the edge (left side in boundary). In contrast, the S element ((white dot) in (d)) was detected far from the edge. Thus, these data suggest that akaganeite was doped onto the PES polymer scaffolds and that the Fe was gradually distributed from the inner area to the edge of the granularity. These data verify the immobilization of the akaganeite particles from the PES polymer scaffolds.

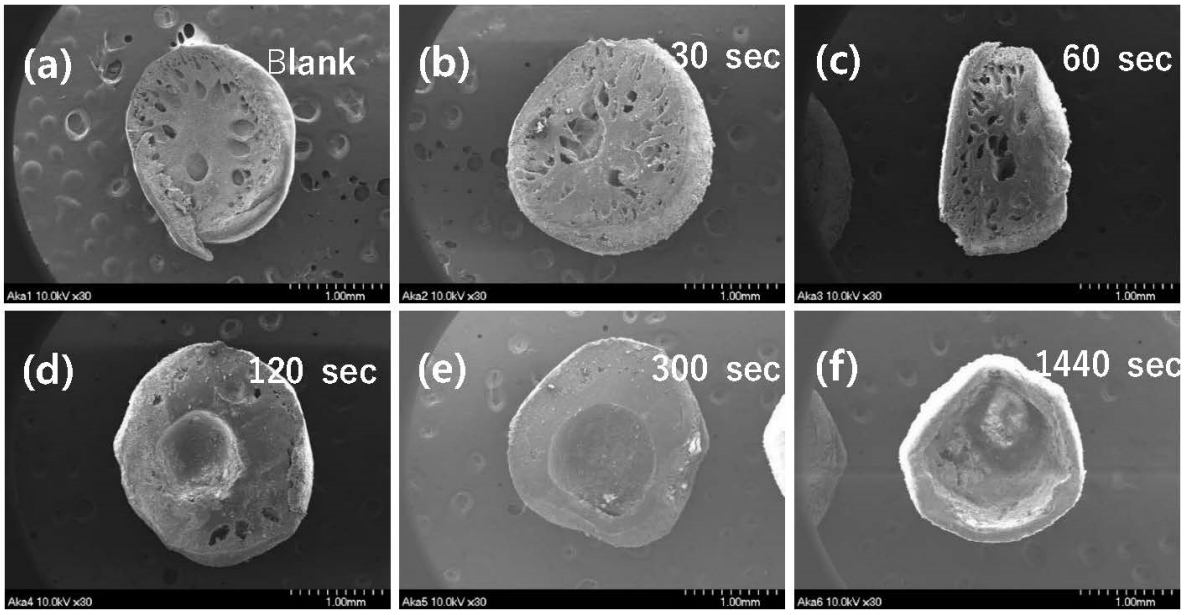

Figure 4. SEM images of cross-section area for synthesized granular akaganeite depending on the exposure time in the air. The samples are named as follows: blank (**a**), 30 s (**b**), 60 s (**c**), 120 s (**d**), 300 s (**e**), and 1440 s (**f**).

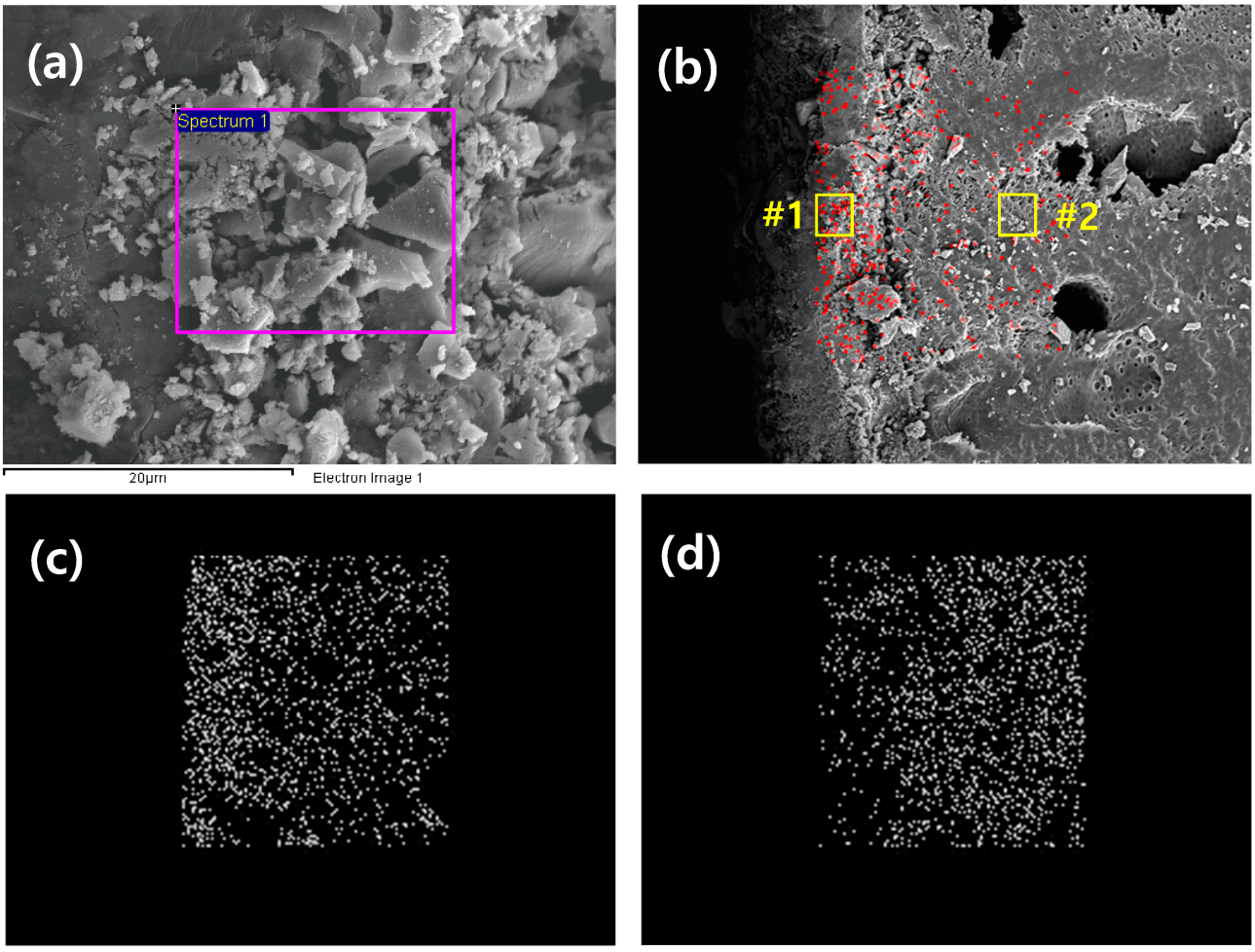

Figure 5. SEM images of cross-sections of granular akaganeite (**a**), EDS mapping of Fe (**b**), EDS mapping of O (**c**) and EDS mapping of S (**d**).

Table 1. The constituent elements from qualitative analysis of the PES polymer and cross-section area on the edge part of granular akaganeite as shown in Figure 5b.

Only PES			#1			#2	
Element	**Weight (%)**	**Atomic (%)**	**Element**	**Weight (%)**	**Atomic (%)**	**Weight (%)**	**Atomic (%)**
C K	53.60	66.36	O K	35.81	64.05	37.50	62.20
O K	26.03	24.20	S K	8.03	7.16	22.97	19.01
S K	20.37	9.45	Fe K	56.17	28.78	39.53	18.78
Total	100.00		Total	100.00		100.00	

3.2.2. TGA Analysis of Granular Iron Oxyhydroxide

TGA profiles of the thermal decomposition were analyzed to determine the PES polymer retention on a granule. First, powdered akaganeite showed weight loss by hydroxyl group decomposition up to 300 °C (Figure 6 (red line)). According to previous studies, akaganeite heated at temperatures above 300 °C transforms into hematite and magnetite [32,33]. Secondly, granular akaganeite showed a substantial weight loss at around 550 °C (Figure 6 (black line)); a substantial amount of PES polymer was volatilized due to the combination of carbon dioxide with the oxygen and carbon atoms. From this result, it is clear that the remaining PES in the granule accounted for approximately a 55% difference, with 86.05% for powdered akaganeite and 31.03% for granule akaganeite, suggesting that 55% of PES polymer was in granule form while the rest in powder form.

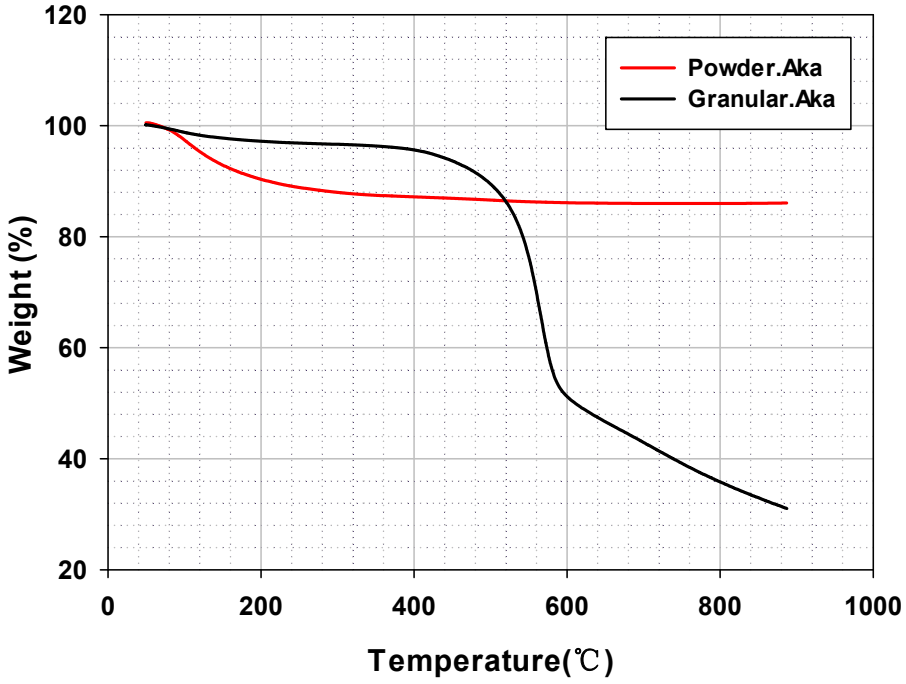

Figure 6. Thermogravimetric analysis curves of powdered/granular akaganeite.

3.2.3. BET Analysis of Granular Iron Oxyhydroxide

The hysteresis loop obtained from granular akaganeite showed type V with mesoporosity. This indicates that the pore shape of akaganeite immobilized onto PES polymer suggests ink-bottle-shaped pores (Figure 7 (blue line)) [29]. Moreover, no difference was identified between the pore sizes of powdered/granular akaganeite (Table 2), implying no structural changes after granulation. However, the BET surface area of granular akaganeite was reduced by 4 times compared with the powdered akaganeite, as suggested by SEM/TGA analysis. Preferentially, the TGA analysis confirmed that half-weight loss of beads was observed in each powdered akaganeite/PES polymer. The outer surface of the bead has an affinity for nitrogen adsorption (Figure 8a), but inner akaganeite immobilized

onto the PES polymer does not contribute towards adsorption due to loss by fixation (Figure 8b). This means that the akaganeite particles were reduced to half. Thus, consideration of the amount of akaganeite in the bead and the effective area on the bead surface could explain why BET surface area had reduced to one-fourth of the adsorption capacity; the analysis accurately corresponded to the 4-fold reduction in surface area (Table 2).

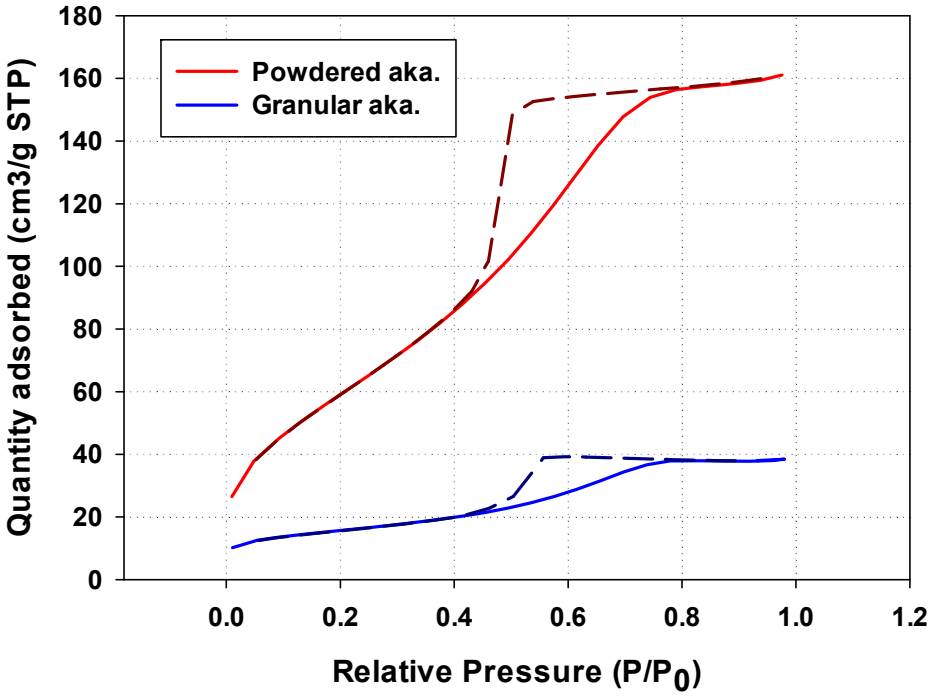

Figure 7. Nitrogen adsorption/desorption isotherm obtained for powdered/granular iron oxyhydroxide.

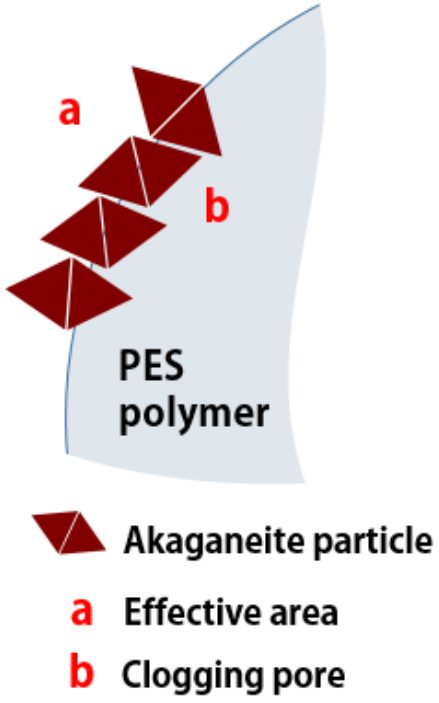

Figure 8. Schematic diagram of pore clogging.

Table 2. Comparison of physical properties of the powdered/granular akaganeite.

	Powdered Akaganeite	Granular Akaganeite
BET surface area (m^3/g)	231	54
Pore volume (cm^3/g)	0.249	0.060
Pore size (nm)	4.3	4.4

3.3. Adsorption Experiments

3.3.1. Kinetic Adsorption/Desorption Experiment

Kinetic adsorption/desorption of phosphate anions by GAK was measured using phosphate 5 mg/L as initial phosphate concentration, followed by desorption of adsorbed granular akaganeite using 50 mL of NaOH 0.5 M. The adsorption kinetic experiment data (Figure 9) were fitted into a pseudo-second-order rate kinetic model, and the rate constants and determination coefficients were tabulated (Figure 9). The adsorption/desorption kinetics indicate that the desorption rate was faster than the adsorption rate due to the strong base of NaOH 0.5 M with a pH range of 13~14. This is supported by the rate constant (k_2). Accordingly, each equilibrium time at 5 mg/L of phosphate was estimated as 12 h for adsorption and 6 h for desorption. Furthermore, the pseudo-second-order kinetic model calculated the equilibrium adsorption capacity (q_e) to be 2.71 mg/g and the desorption capacity to be 2.53 mg/g. The desorption rate was thus estimated to be 93%.

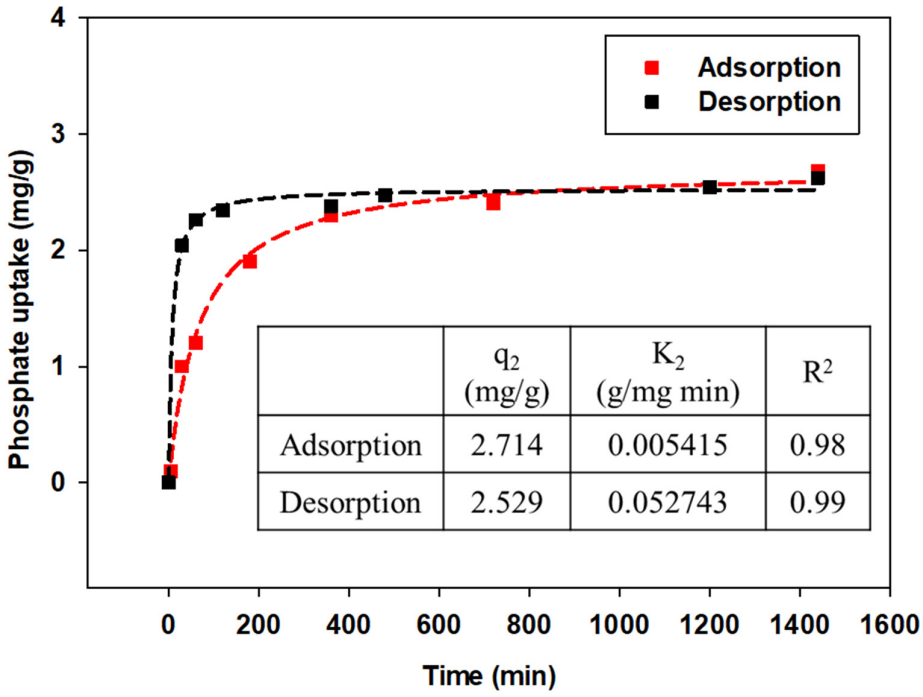

Figure 9. Effect of contact time on the adsorption of phosphate onto granular akaganeite applied by the pseudo-second-order kinetic model.

3.3.2. Isothermal Adsorption Experiment

Experimental data were expressed by q_e (amount of phosphate anions attached to adsorbents) versus Ce (equilibrium concentration of phosphate anions in the solution) plots, and the parameters were calculated by applying Freundlich and Langmuir isotherm models for each powdered/granular akaganeite (Figures 10 and 11). The adsorption isotherm model of powdered/granular akaganeite followed the Freundlich isotherm model with $R^2 > 0.88$ for both powdered and granular akaganeite, using the Sigma plot 12.0 program. This result was analyzed using the Freundlich model with a high R^2. It showed that powdered akaganeite has an affinity for phosphate anions, as shown by $n > 1.0$; conversely, granular akaganeite showed a lower affinity, as shown by $n < 1.0$. The maximum adsorption

capacity was calculated to be 21.27 mg/g for powdered akaganeite and 3.65 mg/g for granular akaganeite. The reason for the lower adsorption capacity of granular akaganeite was that the BET surface area was decreased by the immobilization of the particles from the PES polymer, and only the outer surface had effective adsorption. Thus, it is possible to remove phosphate at a concentration of 5 mg/L, which a biological treatment process cannot remove.

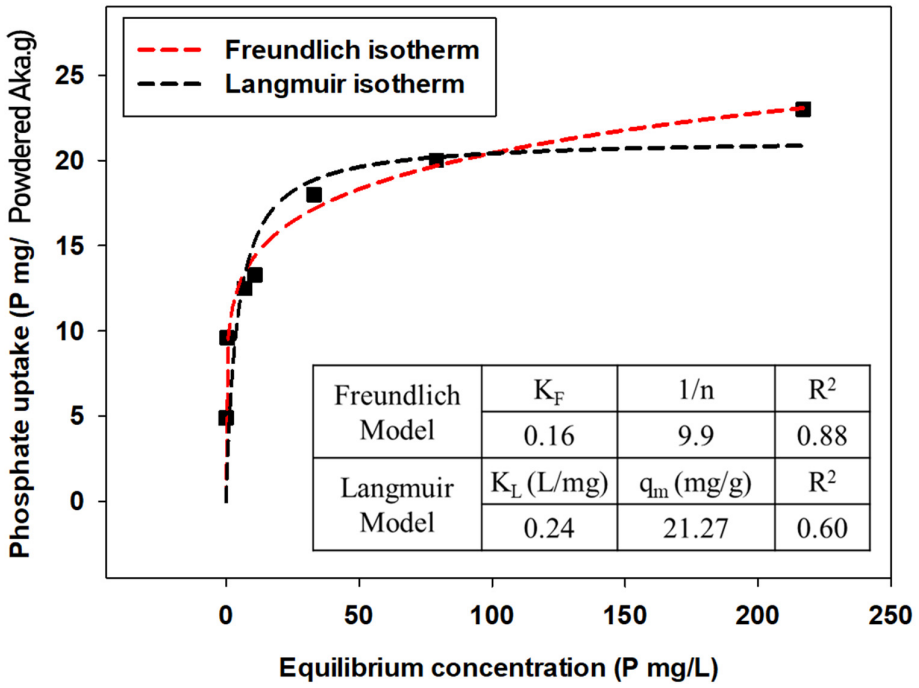

Figure 10. Adsorption isotherms for powdered akaganeite obtained using the Freundlich model (red dash line) and Langmuir model (black dash line).

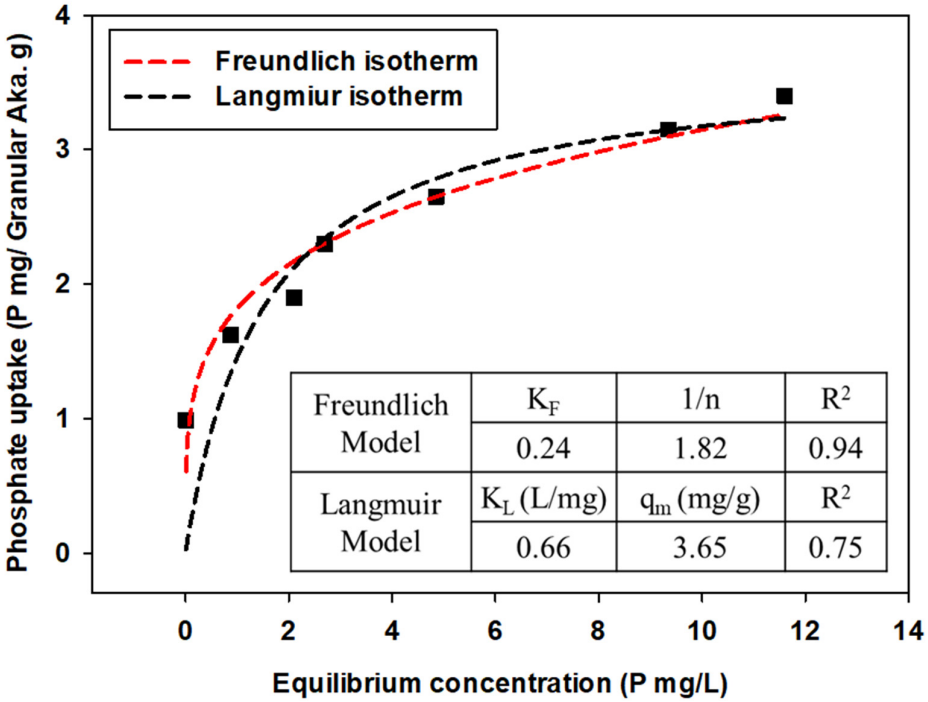

Figure 11. Adsorption isotherms for granular akaganeite obtained using the Freundlich model (red dash line) and Langmuir model (black dash line).

4. Conclusions

In this study, akaganeite with an FeOOH structure in iron oxyhydroxide was synthesized, and reusable materials were developed. Immobilization with the core–shell method using polyethersulfone was applied as a strategy to recover phosphate anions from a trace of phosphate solution. The synthesized granular akaganeite was successfully investigated through various analyses, such as SEM/TGA/BET, to understand its physical properties.

The XRD analysis of the powder form of the synthesized akaganeite showed a blunt peak, while TEM showed an aggregated millet grain shape with an average size of 5 nm. The SAD patterns of akaganeite verified the amorphous form owing to scattering patterns; these data were supported by the results from XRD analysis. Powdered akaganeite had a surface area of 231 mg^2/g and was estimated as a superior material given that the zeta potential of akaganeite was higher than that of goethite and lepidocrocite at pH 6–7, with 5 mg/L of phosphate. In the granulation process, to prevent the dispersion of the powder, granular akaganeite was synthesized using polyethersulfone as a scaffold. The granulation of akaganeite was carried out to improve the field applicability of intrinsic akaganeite. In the analysis of its characteristics, the result of the SEM images of the cross-section area of granular akaganeite depending on the exposure time was explained by the dry phase inversion due to DMF volatility participating in forming holes in an internal granule. SEM/EDS analyses of the edge surface of granular akaganeite suggest that akaganeite particles are well immobilized onto PES polymer scaffolds. Moreover, based on the pore size data, the physical properties were found to have remained unchanged. Finally, the surface area of granular akaganeite decreased by 4–5 times compared to powdered akaganeite. The adsorption kinetic of granular akaganeite was well fitted by the pseudo-second-order model ($R^2 > 0.99$ for adsorption and $R^2 > 0.99$ for desorption). The adsorption equilibrium time for granular akaganeite reached 12 h, while the desorption equilibrium time reached 6 h. Furthermore, the equilibrium adsorption capacity (q_e) was calculated as 2.71 mg/g using the pseudo-second-order kinetic model, while the desorption capacity was calculated as 2.53 mg/g. The Freundlich and the Langmuir isotherm models were applied using granular akaganeite as well.

Powdered akaganeite showed a high removal efficiency in affinity with phosphate anions. On the other hand, granular akaganeite showed a lower affinity. This suggests that the granulation of akaganeite with the PES polymer did not change its adsorption property. As a result, the maximum adsorption capacities calculated were 21.27 mg/g for powdered akaganeite and 3.65 mg/g for granular akaganeite.

Author Contributions: Conceptualization, J.B.; methodology, H.W. and S.K.; validation, S.B. and J.B.; investigation, S.O.; data curation, J.B.; writing—original draft preparation, H.W. and J.B.; writing—review and editing, S.O., S.K. and S.B.; supervision, J.B.; project administration, S.B.; funding acquisition, J.B. All authors have read and agreed to the published version of the manuscript.

Funding: This research was supported by the Korea Ministry of Environment under the Aquatic Ecosystem Conservation Research Program (No. 20230206-001). The authors are very grateful for the funds (Project #20230160-001) provided by the "Korea Institute of Civil Engineering and Building Technology" (KICT), Republic of Korea.

Institutional Review Board Statement: Not applicable for studies not involving humans or animals.

Informed Consent Statement: Not applicable for studies not involving humans.

Data Availability Statement: The data presented in this study are available on request from the corresponding author. The data are not publicly available due to privacy.

Conflicts of Interest: The authors declare no conflicts of interest.

References

1. Bajammal, S.S.; Zlowodzki, M.; Lelwica, A.; Tornetta, P., 3rd; Einhorn, T.A.; Buckley, R.; Leighton, R.; Russell, T.A.; Larsson, S.; Bhandari, M. The use of calcium phosphate bone cement in fracture in treatment: A meta-analysis of randomized trials. *J. Bone Jt. Surg.* **2008**, *90*, 1186–1196. [CrossRef] [PubMed]

2. Putt, M.S.; Milleman, K.R.; Milleman, J.L.; Ghassemi, A. Comparison of a dual-phase fluoride thoothpaste containing calcium, phosphate, and sodium bicarbonate with a regular fluoride thoothpaste on calculus formation. *Compend. Contin. Educ. Dent.* **2004**, *25*, 44–51. [PubMed]
3. Dal'Belo, S.E.; Gaspar, L.R.; Maia Campos, P.M. Moisturinzing effect of cosmetic formulations containing Aloe vera extract in different concentrations assessed by skin bioengineering techniques. *Ski. Res. Technol.* **2006**, *12*, 241–246. [CrossRef] [PubMed]
4. Xu, S.; Zhu, S.; Xiong, H. phosphate adsorption removals by five synthesized isomeric α-, β-, γ-FeOOH. *Water Air Soil Pollut.* **2022**, *233*, 454. [CrossRef]
5. Kalaitzidou, K.; Zouboulis, A.; Mitrakas, M. Thermodynamic study of phosphate adsorption and removal from water using iron oxyhydroxides. *Water* **2022**, *14*, 1163. [CrossRef]
6. Ginebra, M.P.; Espanol, M.; Montufar, E.B.; Perez, R.A.; Mestres, G. New processing approaches in calcium phosphate cements and their applications in regenerative medicine. *Acta Biomater.* **2010**, *6*, 2863–2873. [CrossRef]
7. de Ridder, M.; de Jong, S.; Polchar, J.; Lingemann, S. *Risks and Opportunities in the Global Phosphate Rock Market*; The Hague Centre for Strategic Studies: Hague, The Netherlands, 2012.
8. Jasinski, S.M. *Mineral Commodity Summaries 2011*; U.S. Geological Survey: Reston, VA, USA, 2011.
9. Cooper, J.; Lombardi, R.; Boardman, D.; Carliell-Marquet, C. The future distribution and production of global phosphate rock reserves. *Resour. Conserv. Recycl.* **2011**, *57*, 78–86. [CrossRef]
10. Abu-Obaid, S.; Aktij, S.A.; Tabe, S.; Sadrzadeh, M.; Farnood, R.R. Surfactant-modified adsorptive electrospun nanofiber membrane impregnated with akageneite for phosphorus recovery from wastewater. *J. Environ. Chem. Eng.* **2022**, *10*, 108786. [CrossRef]
11. Wilsenach, J.A.; Schuurbiers, C.A.; van Loosdrecht, M.C. Phosphate and potassium recovery from source separated urine through struvite precipitation. *Water Res.* **2007**, *41*, 458–466. [CrossRef]
12. Kim, S.-J.; Park, T.-J.; Kim, S.-H.; Yang, H.-J. *Characteristics of Residual Metals from Phosphorus Removal in Sewage Treatment Plants around Paldang Lake*; National Institute of Environmental Research in Korea: Incheon, Republic of Korea, 2012.
13. Cheng, W.; Li, J.; Sun, J.; Luo, T.; Marsac, R.; Boily, J.F.; Hanna, K. Nalidixic Acid and Fe (II)/Cu (II) Coadsorption at Goethite and Akaganéite Surfaces. *Environ. Sci. Technol.* **2023**, *57*, 15680–15692. [CrossRef]
14. Boparai, H.K.; Joseph, M.; O'Carroll, D.M. Kinetics and thermodynamics of cadmium ion removal by adsorption onto nano zerovalent iron particles. *J. Hazard. Mater.* **2011**, *186*, 458–465. [CrossRef] [PubMed]
15. Altundogan, H.S. Cr (VI) removal from aqueous solution by iron (III) hydroxide-loaded sugar beet pulp. *Process Biochmistry* **2005**, *40*, 1443–1452. [CrossRef]
16. Phuengprasop, T.; Sittiwong, J.; Unob, F. Removal of heavy metal ions by iron oxide coated sewage sludge. *J. Hazard. Mater.* **2011**, *186*, 502–507. [CrossRef] [PubMed]
17. Gong, J.-L.; Wang, X.-Y.; Zeng, G.-M.; Chen, L.; Deng, J.-H.; Zhang, X.-R.; Niu, Q.-Y. Copper (II) by pectin-iron oxide magnetic nanocomposite adsorbent. *Chem. Eng. J.* **2012**, *185–186*, 100–107. [CrossRef]
18. Gu, B.; Lian, L.; Dickey, J.; Yin, X.; Dai, S. Reductive precipitation of uranium (VI) by zero-valent iron. *Environ. Sci. Technol.* **1998**, *32*, 3366–3373. [CrossRef]
19. Hanesch, M. Raman spectroscopy of iron oxides and (oxy)hydroxides at low laser power and possible application in environmental magnetic studies. *Geophys. J. Int.* **2009**, *177*, 941–948. [CrossRef]
20. Navrotsky, A.; Mazeina, L.; Majzlan, J. Size-driven structural and thermodynamic complecity in iron oxides. *Science* **2008**, *319*, 1635–1638. [CrossRef]
21. Kim, J.; Li, W.; Philipsc, B.L.; Grey, C.P. Phosphate adsorption on the iron oxyhydroxides goethite (α-FeOOH), akaganeite (β-FeOOH), and lepidocrocite (γ-FeOOH): P NMR study. *Energy Environ. Sci.* **2011**, *4*, 4298–4305. [CrossRef]
22. Chitrakar, R.; Tezuka, S.; Sonoda, A.; Sakane, K.; Ooi, K.; Hirotsu, T. Phosphate adsorption on synthetic goethite and akaganeite. *J. Colloid Interface Sci.* **2006**, *298*, 602–608. [CrossRef]
23. Li, N.; Bai, R. Copper adsorption on chitosan-cellulose hydrogel beads: Behaviors and mechanisms. *Sep. Purif. Technol.* **2005**, *42*, 237–247. [CrossRef]
24. Chang, J.; Woo, H.; Ko, M.S.; Lee, J.; Lee, S.; Yun, S.T.; Lee, S. Targeted removal of trichlorophenol in water by oleic acid-coated nanoscale palladium/zero-valent iron alginate beads. *J. Hazard. Mater.* **2015**, *293*, 30–36. [CrossRef] [PubMed]
25. Grisdanurak, N.; Akewaranugulsiri, S.; Futalan, C.; Tsai, W.-C. The study of copper adsorption from aqueous solution using crosslinked chitosan immobilized on bentonite. *J. Appl. Polym. Sci.* **2012**, *125*, 132–142. [CrossRef]
26. Liu, R.; Guo, Y.; Odusote, G.; Qu, F.; Priestley, R.D. Core-shell Fe_3O_4 polydopamine nanoparticles serve multipurpose as drug carrier, catalyst support and carbon adsorbent. *ACS Appl. Mater. Interfaces* **2013**, *5*, 9167–9171. [CrossRef] [PubMed]
27. Li, J.-F.; Xu, Z.-L. Effect of TIO_2 nanoparticles on the surface morphology performance of microporous PES membrane. *Appl. Surf. Sci.* **2009**, *255*, 4725–4732. [CrossRef]
28. Song, X. Surface and Bulk Reactivity of Iron Oxyhydroxides: A Molecular Perspective. Ph.D. Thesis, Umeå University, Umeå, Sweden, 2013.
29. Jemutai-Kimosop, S.; Okello, V.A.; Shikuku, V.O.; Orata, F.; Getenga, Z.M. Synthesis of mesoporous akaganeite functionalized maize cob biochar for adsorptive abatement of carbamazepine: Kinetics, isotherms, and thermodynamics. *Clean. Mater.* **2022**, *5*, 100104. [CrossRef]
30. Klaysom, C.; Moon, S.-H.; Ladewig, B.; Lu, G.Q.; Wang, L. Preparation of porous ion-exchange membranes (IEMs) and their characterizaotns. *J. Membr. Sci.* **2011**, *371*, 37–44. [CrossRef]

31. Wen, S.; Lu, Y.; Dai, J.; Huang, X.; An, S.; Liu, J.; Liu, Z.; Du, Y.; Zhang, Y. Stability of organic matter-iron-phosphate associations during abiotic reduction of iron. *J. Hazard. Mater.* **2023**, *449*, 131016. [CrossRef]
32. Asenath-Smith, E.; Estroff, L.A. Role of Akaganeite (β-FeOOH) in the Growth of Hematite (α-Fe_2O_3) in an inorganic silica hydrogel. *Cryst. Growth Des.* **2015**, *15*, 3388–3398. [CrossRef]
33. Choi, J.; Cha, J.; Lee, J.-K. Synthesis of various magnetite nanoparticles through simple phase transformation and their shape dependent magnetic properties. *RSC Adv.* **2013**, *3*, 8365–8371. [CrossRef]